The magnetism measurements of the two-dimensional van der Waals antiferromagnet $CrPS_4$ using dynamic cantilever magnetometry.

Qi Li,[†,‡,‖] Weili Zhen,[†,‖] Ning Wang,[†,‖] Yang Yu,[¶] Senyang Pan,[†,‡] Lin Deng,[†,‡] Jiaqiang Cai,[†,‡] Kang Wang,[*,†] Lvkuan Zou,[*,§] Zhongming Zeng,[§] Jinglei Zhang,[*,†] and Haifeng Du[†]

†*Anhui Province Key Laboratory of Condensed Matter Physics at Extreme Conditions, High Magnetic Field Laboratory, HFIPS, Anhui, Chinese Academy of Sciences, Hefei 230031, People's Republic of China*

‡*University of Science and Technology of China, Hefei 230026, People's Republic of China*

¶ *School of advanced manufacturing engineering Hefei university Hefei 230601*

§*Suzhou Institute of Nano-techand Nano-bionics,Chinese Academy of Sciences,Suzhou215123,P. R.China*

‖*These authors contributed equally to this work.*

E-mail: kwang@hmfl.ac.cn; lkzou2023@sinano.ac.cn; zhangjinglei@hmfl.ac.cn

Abstract

The exploration of van der Waals (vdWs) magnetic materials has sparked great interest in spintronics. However, conventional methods often face challenges in characterizing the magnetic properties of small-sized vdWs materials, especially for antiferromagnets with extremely small magnetic moments. Here, we demonstrate the efficacy of dynamic cantilever magnetometry (DCM) in characterizing the magnetic properties of

vdWs magnets, using an antiferromagnetic semiconductor $CrPS_4$. We observe continuous spin axis rotation under a magnetic field, accurately modelled by considering the existance of marked magnetic anisotropies. Furthermore, the dominance of out-of-plane magnetic anisotropy in spin reorientation behavior at low temperatures transitions to the prevalence of in-plane anisotropy with increasing temperature, leading to a sign reversal of the frequency shift in measurements. The peculiar magnetic phase transitions make $CrPS_4$ an intriguing platform for studying two-dimensional magnetism. Our findings underscore the effectiveness of DCM in characterizing magnetic anisotropies and phase transitions in vdWs magnets.

Introduction

The investigation of van der Waals (vdWs) magnetic materials has ignited significant enthusiasm in the field of spintronics.[1–6] Directly acquiring magnetization and analyzing magnetic anisotropies are essential for understanding novel phenomena,[7–9] such as nontrivial magnetizing behavior,[10] magnetic phase transitions[11,12] and hidden orders.[13,14] However, there are limited research having been conducted on magnetization measurement in cleavable vdWs materials primarily due to the stringent sensitivity requirements that are seldom met by commercial devices. The total magnetic moment in vdWs magnets is usually extremely small, particularly for vdWs antiferromagnets. Advanced techniques such as the vibrating sample magnetometry,[15] magnetic force microscopy,[16] and magneto-optic Kerr effect microscopy[7] have limited sensitivity in measuring magnets with extremely small magnetic moments. For example, vibrating sample magnetometry has a sensitivity of $10^{-9} A \cdot m^2$ for magnetization measurement. This poses challenges as it typically requires a large volume of magnetic samples, impeding the study of magnetic properties within atomic-layer thicness. Therefore, developing an advanced technique for highly sensitive measurement of vdWs magnetic materials is essential.

Emerging Dynamic Cantilever Magnetometry (DCM) has previously been demonstrated

as a technique with ultrahigh sensitivity, reaching $10^{-17} A \cdot m^2$.[17,18] While this sensitivity enables the measurement of magnetization in various individual nano-scale samples,[18,19] its application specifically in vdWs thin magnets has not yet been demonstrated. When a nanometer-sized material is mounted onto the free end of a cantilever, an external magnetic field alters the magnetotropic coefficient, resulting in variations in effective stiffness. The magnetization in such a thermodynamic system can be revealed by monitoring the eigen-frequency shifts of the cantilever. Conventional DCM devices with sophisticated structures have long been fabricated using focused ion beam (FIB). However, for vdWs materials, FIB-induced surface damage may lead to moment loss.

In this work, we develop a clean fabrication technique for assembling DCM devices to characterize the intrinsic magnetic properties of vdWs thin films. Using the vdWs antiferromagnetic semiconductor $CrPS_4$ as our focus, we demonstrate the effectiveness of DCM in characterizing the magnetic properties of vdWs magnets, even when dealing with extremely small magnetic moments. $CrPS_4$, a ternary transition metal chalcogenide (TTMC), has monoclinic symmetry with space group C2/m.[20] The closely packed surface is constituted by S atoms in monolayers as presented in figure 1(a).[21] Magnetically, $CrPS_4$ exhibits intralayer ferromagnetism and weak interlayer antiferro-coupling.[22,23] These intricate magnetic interactions make $CrPS_4$ a promising vdWs magnets with various intriguing properties, such as synaptic effect,[24] giant tunneling magnetoresistance,[25,26] and exchange bias effects.[27] Additionally, these magnetic interactions, along with magnetic anisotropies, contribute to a complex phase transition accompanied by continuous spin axis rotation under a magnetic field. The exceptionally weak magnetic moments and the intriguing magnetic phase transitions of $CrPS_4$ position it as a naturally superior candidate for demonstrating the capability of DCM in examining the magnetism of few-layered two-dimensional magnets. We accurately model the spin reorientation behavior using a spin-flopping model. Furthermore, we uncover a sign reversal of the frequency shift in measurements with varying temperatures, attributed to the transition from out-of-plane magnetic anisotropy dominance at low tem-

peratures to in-plane anisotropy dominance at high temperatures. These findings underscore the capability of DCM in elucidating magnetic anisotropies and phase boundaries in vdWs magnets.

Results and discussion

The vdWs interactions between layers of $CrPS_4$ allow mechanical exfoliation down to atomic level. Before exfoliation, We prepared $CrPS_4$ crystals and performed preliminary crystal characterization using x-ray diffraction, as presented in supplementary figure. Furthermore, we also conducted zero-field-cooled (ZFC) magnetization measurements both in-plane and out-of-plane (at $\mu_0 H = 0.1T$) as illustrated in figures 1(b) and 1(c). Results demonstrate a Néel temperature T_N of approximately 38K in bulk $CrPS_4$, consistent with previous studies.[20] The feature observed at around 34.7K in figure 1(c) may reveal realignments of spins.

To investigate magnetization in few layered and small-sized $CrPS_4$, while safeguarding the sample from damage, we devised a pristine fabrication technique for assembling DCM devices. It is worth noting that this technique is not limited to vdWs materials. Rather, it is also well-suited for other small-sized materials. Experimentally, we mechanically exfoliated the$CrPS_4$ and utilize ethonal to reduce the intermolecular forces between thin film and the substrate. Subsequently, we used micro manipulators to transfer few-layered $CrPS_4$ onto the free end of the cantilever as schematically presented in figure 1(d). Figure 1(e) illustrates the scanning electron microscope (SEM) image of the DCM device 1 (D1), which consists of a cantilever with a thickness of 200 nm, a length of 200 μm, and a width of 10 μm. The octagonal pad of the cantilever was designed to facilitate sample mounting and laser return. As depicted in figure 1(f), a thin film with a lateral size less than 35 μm^2 and thickness of approximately 200 nm was affixed to the backside of the pad.

To reveal the magnetization of the small-sized $CrPS_4$, DCM measurements were conducted while sweeping the magnetic field in the z-direction. The DCM device was sealed in

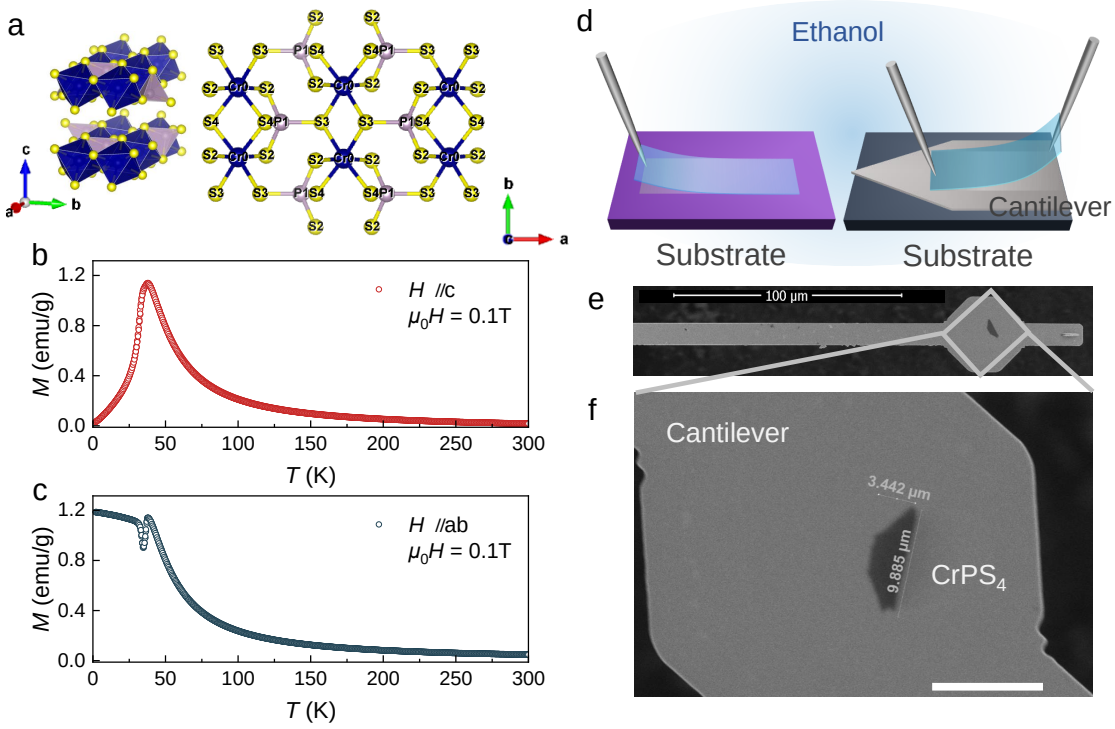

Figure 1

Characterization of $CrPS_4$ and presentation of the DCM device. (a) The crystal structure of $CrPS_4$. (b) and (c) depict the c-direction and ab-plane magnetic susceptibilities, respectively, measured under a magnetic field of $\mu_0 H = 0.1T$. (d) Schematic representation of ethanol-assistant transfer of 2D $CrPS_4$. Gray needles represent stretched glass capillaries for transfer. The entire experiment was conducted in an alcohol environment (transparent dark blue). (e) Scanning electron microscope (SEM) image of the DCM device with a thickness of 200 nm and a length of 200 μm. (f) Zoom-in illustration of the pad with the sample mounted on it (Scale bar: 10μm).

a vacuum sleeve, maintaining a pressure below 10^{-6} mbar, to minimize vibration dissipation. The D1 exhibited eigen frequency f_0 of 4.3 kHz, monitored by a home-made laser interferometer. The laser interferometer enables the detection of the cantilever's displacement to less than 1 nm. This, together with the utilization of a cantilever with low stiffness and high quality factor, ensures the high sensitivity of magnetization measurements.

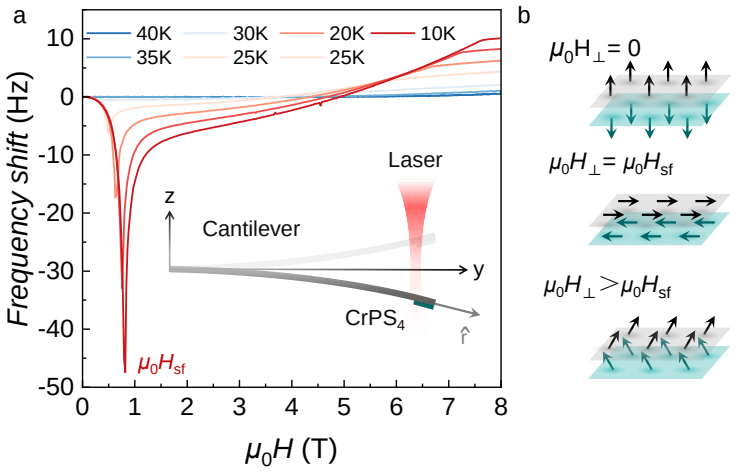

Figure 2
DCM measurements in the D1. (a) The frequency shift of the D1 in DCM measurements at selected temperatures. Inset in (a) schematically illustrates the experimental setup. The cantilever is securely fixed along the y-axis and vibrates within y-z plane. The laser is directed along the z-axis. (b) The deduced magnetic structure in metamagnetic phase transition of $CrPS_4$ below 35K.

To investigate the magnetizing behavior of $CrPS_4$, we measured the frequency shift Δf as a function of the magnetic field μ_0H from 5K to 40K, as shown in figure 2(a). DCM results present a two-stage transition. The data at 5 K show that Δf significantly drops until reaching a minimum around 0.8 T, followed by an upward trend from rapid to gradual increase and ultimately transitioning to a linear region with a change in slope. The discontinuity in Δf is consistent with a spin-flop transition (with a spin flop field $\mu_0 H_{sf}$). We consider two sets of spin alignments in sublattices (green and black arrows in figure 2(b)). The alignments maintain arrangement along the easy axis in the absence of an external magnetic field. When the out-of-plane field reaches $\mu_0 H_{sf}$, the in-plane arrangement exhibits relatively lower

energy and the Néel vector prefers to flop into the a-b plane. Above $\mu_0 H_{sf}$, the Néel vector undergoes a gradually rotation from the a-b plane to the external field, exhibiting a canted layered antiferromagnetic alignment.

To understand the magnetizing progress, we consider the free energy of the system

$$E = \frac{1}{2}k_0 l_\theta^2 \theta^2 - M_a V H \cos(\phi_a - \theta) - M_b V H \cos(\phi_b - \theta) + \frac{1}{2}KV\left(\sin^2\phi_a + \sin^2\phi_b\right) + AM_a M_b V^2 \cos(\phi_a - \phi_b). \quad (1)$$

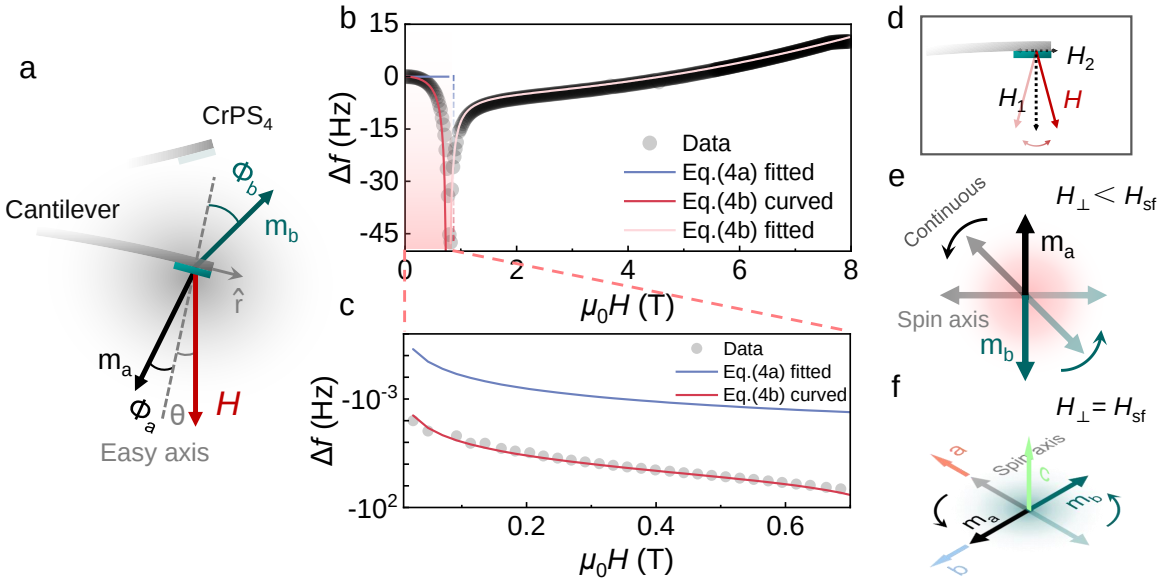

Figure 3
(a) Schematic view of the relative orientations of the cantilever axis, applied magnetic field H, and magnetic moments in sublattices. (b) The measurements of Δf were obtained while sweeping H in the z direction. Below the spin flop field, data fitting was performed using the uniaxial model (light blue) and flopping function (light red). Detailed disparities in zoom-in view (c) shows a more suitable fit between data (gray circles) and the flopping function (light red line). (d) The relative direction of magnetic field while treating cantilever as a static system. The corresponding putative magnetic arrangements in sublattices below (or reach) spin flop field are shown in (e) (or (f)).

The k_0 and l_θ represent the inherent stiffness and effective length of cantilever. Here, we treat the anisotropy constant as K and antiferromagnetic interaction as A. θ depicts the vibration deviation, which induces instantaneous alignments M_a and M_b at angles ϕ_a and ϕ_b, respectively, to the easy axis in sublattices. For a sample with volume of V resided in

equilibrium, we have

$$\begin{aligned}\frac{\partial E}{\partial \phi_n} &= M_a V H \sin(\phi_a - \theta) + \frac{1}{2} K V \sin 2\phi_a - A M_a M_b V^2 \sin(\phi_a - \phi_b) = 0 \\ \frac{\partial E}{\partial \phi_n} &= M_b V H \sin(\phi_b - \theta) + \frac{1}{2} K V \sin 2\phi_b + A M_a M_b V^2 \sin(\phi_a - \phi_b) = 0,\end{aligned} \tag{2}$$

and $\frac{\partial^2 E}{\partial {\phi_a}^2} > 0$, $\frac{\partial^2 E}{\partial {\phi_b}^2} > 0$. Then considering the instantaneous vibration $\theta \ll 1$, one can get

$$\begin{aligned}\theta &= \frac{M_a H \sin\phi_a + \frac{1}{2} K \sin 2\phi_a - A M_a M_b V \sin(\phi_a - \phi_b)}{M_a H \cos\phi_a} \\ &= \frac{M_b H \sin\phi_b + \frac{1}{2} K \sin 2\phi_b + A M_a M_b V \sin(\phi_a - \phi_b)}{M_b H \cos\phi_b}.\end{aligned} \tag{3}$$

We treated the deflection angle $\phi_i = \phi_a, \phi_b$ of spin as a function around $\theta = 0$ and expend to first order as $\phi_i(\theta) = \phi_{i_0} + \left(\frac{\partial \phi_i}{\partial \theta}\right)_{\theta=0} \theta$, with $\left(\frac{\partial \phi_i}{\partial \theta}\right)_{\theta=0} = 1/\left(\frac{\partial \theta}{\partial \phi_i}\right)_{\phi_i = \phi_{i_0}}$ $(i = a, b)$. We also considered equality of two sets of magnetization, denoted as M_0. The effective stiffness constant is then magnetization-related, denoted by $k = k_0 l_\theta^2 + \sum_i KV \cos 2\phi_{i_0} \left(\frac{\partial \phi_i}{\partial \theta}\right)_{\theta=0}$ $(i = a, b)$, which leads to the frequency shift

$$\Delta f = \frac{\omega_0}{4\pi k_0 l_0^2} \left(\frac{HKM_0}{K + HM_0 + AM_0^2 V} - \frac{HKM_0}{K - HM_0 + AM_0^2 V}\right), \text{for } |H| < H_{sf} \tag{4a}$$

$$\Delta f = \frac{\omega_0}{4\pi k_0 l_0^2} \frac{2M_0 HK \left(\frac{2H^2 M_0^2}{(-K + 2AVM_0)^2} - 1\right)}{M_0 H + (K - AVM_0^2) \left(\frac{2M_0 H}{-K + 2AM_0^2} - \frac{-K + 2AM_0^2}{M_0 H^2}\right)}, \text{for } |H| > H_{sf}. \tag{4b}$$

We fitted the data above the spin-flop transition field $\mu_0 H_{sf}$, leading us to obtain the fitted parameters (light red line). Then we re-positioned the fitted parameters, K and M_0, within the Eq.(4a) to accommodate the low-field range. The resulting fit, referred to as the uniaxial fitting curve (blue lines in figure 3(b) and (c)), which depicts that spin axis undergoes minimal rotation due to the inability of external fields to disrupt the equilibrium. One can observe that the rate of decrease in experiments was excessively rapid compared to the fitting curve before spin-flop transition. Yet the part of data exhibits well-fitted curve using Eq.(4b)

(red line). The significant decline in the observed data suggests a transformation in the magnetic structure, indicating a spin-flop phenomenon where Néel gradually rotates towards the ab-plane rather than undergoing an abrupt transition. These findings further support the results of neutron scattering, which indicates a spin-axis rotation from a-c plane to the b axes likely caused by local anisotropy that constituted by a slightly distorted structure in S anions chains. This phenomenon could be hardly observed in c-direction susceptibility measurements.

The difference between DCM and direct susceptibility measurements lies in the fact that torque provides more information in multiple directions. To be more specific, the torque under a z-direction magnetic field can be expressed as $\tau = \tau_0 + k_0 l_e^2 \theta + m_{\parallel} \cdot H_{\perp} - \chi_{\perp} V$ $H_{\perp} \cdot H_{\parallel}$, which could be reformulated as a first-order Taylor expansion, $\tau_0 + k_0 l_e^2 \theta + m_{\parallel} H\theta - \chi_{\perp} V H\theta \cdot H$. Apart from the kinetic term $k_0 l_e^2$, the differential torque, corresponding to the first order term of θ, uncovers two sources of magnetotropic coefficient. $\chi_{\perp} V H_{\perp} \cdot H_{\parallel}$ arises from the magnetization undergoing a vibrational field (shown in figure 3(d)) induced by the harmonic oscillation of cantilever, while the ohter part, $m_{\parallel} \cdot H_{\perp}$, reveals a restoring force caused by swaying magnetization. The latter depicts an instantaneous magnetizing, which indicates the stability of the current magnetizing state.

To gain a deeper insight into the magnetization of $CrPS_4$, we further performed DCM measurements using another device (D2), featuring a cantilever with dimensions of $500\mu m \times 100\mu m \times 2\mu m$ and precisely defining the arrangement order of the CrPS4 flack on the cantilever. As shown in figure 4(a), the sample exhibits clear edges and characteristic angles with a crystallographic angle of 67.5 deg shown in figure 4(a), which implies that the direction of cantilever is between the a and b axes. To capture the entire magnetizing process, the a and b axes were intentionally designed to be non-parallel with the cantilever.

We carried out field-dependent DCM measurements at different temperatures to illustrate the phase diagram of the $CrPS_4$ flake. As summarized in figure 4(c), four regions were identified, respectively representing different magnetic structures. The spin-flop transition

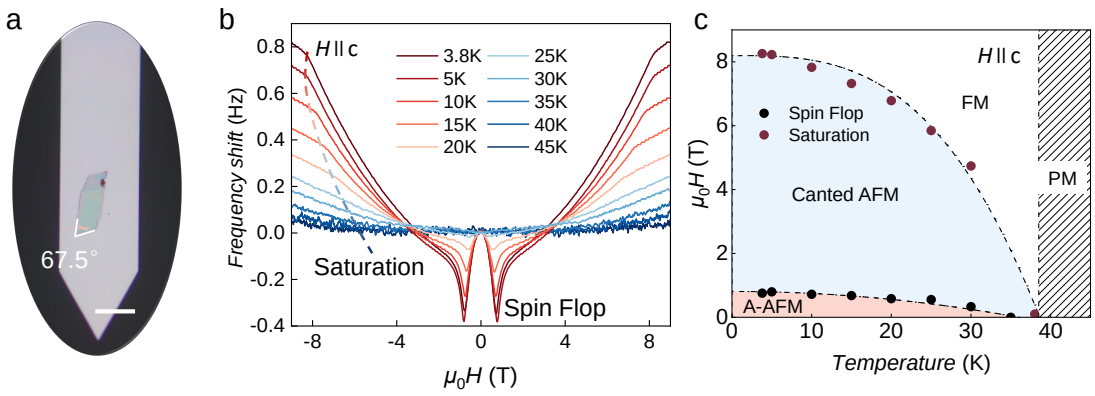

Figure 4
(a) The optical image of DCM device (Scale bar: 50μm). The angle between the two white lines demonstrates its distinct crystal characteristic, measuring 67.5°. (b) Out-of-plane field-dependent frequency shift in DCM results at selected temperatures. The dotted line represents co-linear arrangements of two alignments, corresponding magnetic phase diagram shown in (c). The dark block dots represents spin flop happening and dark red circle dots signify the two alignments rotate to one direction.

field and the saturation field gradually decrease with increasing temperature until reaching the Néel temperature $T_{\mathrm{N}} = 38\mathrm{K}$. Although this result reveals the metamagnetic phase transitions as previously reported in bulk $CrPS_4$, yet the role of magnetic anisotropy in these phase transition remain elusive.

To elucidate the impact of magnetic anisotropy on the phase transition, we further performed DCM measurements by rotating the DCM stage at a 90-deg with the magnetic field in-plane. At a low temperature of 3.8K, wherein the out-of-plane magnetic anisotropy dominates, the frequency shift Δf gradually increases. As external field goes up to a critical value at around 2T, Δf reaches its maximum followed by a decrease and, ultimately reaches its saturation. We noted that the sign of the frequency shift is opposite to that depicted in figure 3 and figure 4. As external field raises up, the angle between the spin and the c axis, leading to a canted alignment. This is different from the spin-flop transition process when applying an out-of-plane magnetic field.

We summarized the data at different temperature in figure 5(a) and (b). Both the Δf and the saturation field decrease with increasing temperature, suggesting decreased

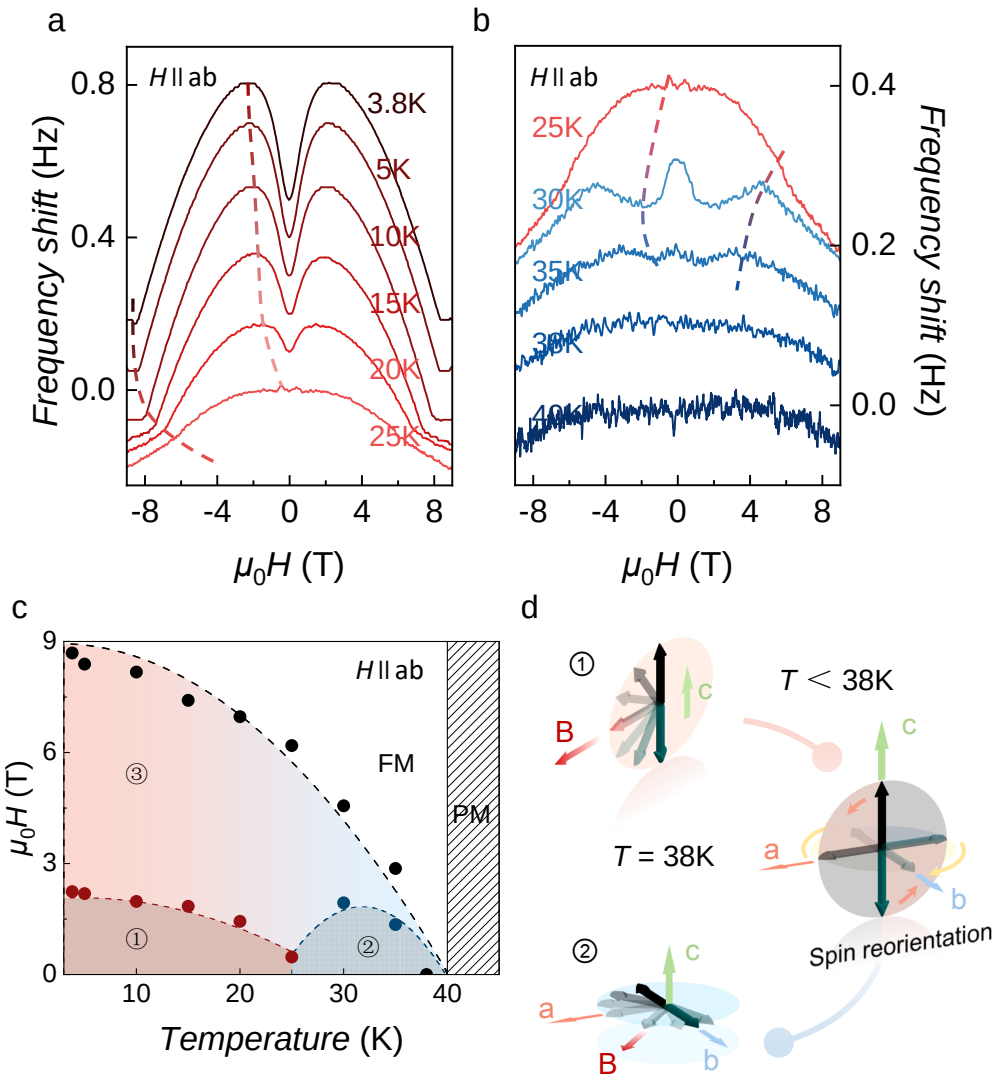

Figure 5
Characterization of in-plane magnetization using DCM measurements. (a) and (b) illustrate the frequency shifts above and below 25K, the dotted line mark the boundaries of co-linear alignments. The corresponding phase diagram has been shown in (c), and putative spin alignments are sketched in (d).

anisotropy and antiferromagnetic coupling. Notebly, when the temperature reaches around 30K, the frequency shift reverses its sign around zero field. Considered by the $\tau = \tau_0 + k_0 l_e^2 \theta + m_{\parallel} \cdot H_{\perp} - \chi_{\perp} V H_{\perp} \cdot H_{\parallel}$, this result suggests an amplitude switching between the y- and z-directions magnetic susceptibilities. At low temperatures, the out-of-plane magnetic anisotropy dominates the spin reorientation transition, while it transitions to the dominance of in-plane anisotropy at high temperature, leading to a sign reversal of Δf. This evidence depicted a magnetized schematic diagram in figure 5(d). The spin alignments prefer to stay out-of-plane below 25K. As system reaches 30K, spin alignments re-orientate from c axis to ab plane, Under an external magnetic field, spin alignments rotate from the b axis to the external field. Also, above T_N, paramagnetic like frequency shifts have been observed.

Importantly, stiffness are second order differential of free energy, which leads to a sensitive response to phase transition. Developing DCM technology is crucial for detecting phase boundaries, exploring hidden orders or providing unambiguous evidence for novel physical phenomena in low-dimensional region.

In summary, we developed an ethanol-assistant transfer technique to prepare DCM devices for small-sized vdWs magnets characterizing the magnetization of $CrPS_4$, which dressed the issue of damage encountered in traditional FIB-fabricated devices. Using this technique, we characterized small-sized $CrPS_4$. We observe a spin-flop transition in the magnetization under an out-of-plane magnetic field. This phenomenon is effectively captured by a macrospin model wherein the inter-layer antiferromagnetic coupling and the marked magnetic anisotropies are considered. Moreover, we identified a transition from the dominance of out-of-plane anisotropy in the spin-reorientation behavior at low temperatures to the dominance of in-plane anisotropy at high temperatures. These unique magnetic phase transitions make $CrPS_4$ as an intriguing platform for studying two-dimensional magnetism. Our findings also demonstrate that the DCM technique is well-suited for characterizing two-dimensional vdWs magnets even with extremely small magnetic moments.

Methods

Preparing the cantilever

First, a thin film of SiO_2 with thickness of 1 μm was grown on top Si layer of a Silicon-on-Insulator (SOI) substrate by plasma-enhanced chemical vapor deposition (PECVD) to balance stress beneath. Patterns of cantilevers were micro-fabricated by ultra-violet lithography on top surface of SOI. An inductively coupled plasma (ICP) deep reactive ion etch (DRIE) was adopted to etch SOI to buried oxide (BOX) layer. On bottom surface of SOI substrate, the patterned 500 μm silicon was removed by DRIE (Bosch Process) on a deep silicon etcher system. Finally, sacrificial SiO_2 layer was released by dry release etch using vapor HF chemistries (sacrificial vapor release etching).

DCM measurements

In measuring, cantilever was mounted onto the DCM stage. Laser of 1550nm passed through the polarization-maintaining optical fiber and focused on the cantilever as a Gaussian beam. The reflected light from the surface of cantilever met the incident laser, and interference happened. The interference light was captured by photodiode (PD) and converted into electrical signal. Through FFT analysis, we obtained the power-density spectrum and identified various peaks. Then ring-down control was utilized to monitor the resonant frequency of cantilever. DCM measuring was carried out in Janis 9T magnet. In order to reduce the dissipation, we sealed the insert and kept pressure below $10^{-6} mbar$.

Experimental

Assembling of DCM device

To assemble DCM devices, ethanol has been used to reduce the intermolecular forces between thin film and the substrate. Experimentally, $CrPS_4$ thin film was mechanically exfoliated

from the bulk crystal and transferred onto a Si substrate. The sample of appropriate size was selected and, together with its substrate, was immersed in ethanol. Here the long focal-length microscope was used to facilitate manipulation in transferring. By monitoring the target area in optical microscope, we gently lifted the sample from a corner until the sample was completely detached from the substrate, by utilizing home-made micromanipulator with a microinjection needle as a manipulator. We then operated multi-axis transfer stage to move the needle above the cantilever at an ultra-slow speed. With the aid of another needle, gentle pressure can be applied to the extremity of the sample attached with the cantilever and subsequently remove the first needle. Finally we checked the device and drained the ethanol.

Acknowledgement

This work was financially supported by the National Key R&D Program of the MOST of China (Grant No. 2022YFA1602602, 2022YFA1403603), the Natural Science Foundation of China (Grants No. 12122411, 12241406), the Strategic Priority Research Program of the Chinese Academy of Sciences (CAS) (Grant No. XDB33030100), CAS Project for YoungScientistsin BasicResearch,GrantNo. YSBR-084, HFIPS Director's Fund (Grants No. 2023BR, YZJJ-GGZX-2022-03, YZJJ202403-TS), the National Natural Science Funds for Distinguished Young Scholar, Grants No. 52325105; and the Equipment Development Project of Chinese Academy of Sciences (Grant No. YJKYYQ20180012,YJKYYQ20180059), HFIPS Director's Fud (Grant No. BJPY2021B05)

References

(1) Bonilla, M.; Kolekar, S.; Ma, Y. J.; Diaz, H. C.; Kalappattil, V.; Das, R.; Eggers, T.; Gutierrez, H. R.; Phan, M. H.; Batzill, M. *Nature Nanotechnology* **2018**, *13*, 289–+

(2) Deng, Y. J.; Yu, Y. J.; Song, Y. C.; Zhang, J. Z.; Wang, N. Z.; Sun, Z. Y.; Yi, Y. F.; Wu, Y. Z.; Wu, S. W.; Zhu, J. Y.; Wang, J.; Chen, X. H.; Zhang, Y. B. *Nature* **2018**, *563*, 94–+

(3) Gong, C.; Zhang, X. *Science* **2019**, *363*, 706–+

(4) Jones, A. M.; Yu, H. Y.; Ross, J. S.; Klement, P.; Ghimire, N. J.; Yan, J. Q.; Mandrus, D. G.; Yao, W.; Xu, X. D. *Nature Physics* **2014**, *10*, 130–134

(5) Wang, Z. et al. *Nature Nanotechnology* **2018**, *13*, 554–+

(6) Zhong, D.; Seyler, K. L.; Linpeng, X. Y.; Cheng, R.; Sivadas, N.; Huang, B.; Schmidgall, E.; Taniguchi, T.; Watanabe, K.; McGuire, M. A.; Yao, W.; Xiao, D.; Fu, K. M. C.; Xu, X. D. *Science Advances* **2017**, *3*

(7) Gong, C.; Li, L.; Li, Z. L.; Ji, H. W.; Stern, A.; Xia, Y.; Cao, T.; Bao, W.; Wang, C. Z.; Wang, Y. A.; Qiu, Z. Q.; Cava, R. J.; Louie, S. G.; Xia, J.; Zhang, X. *Nature* **2017**, *546*, 265–+

(8) Haastrup, S.; Strange, M.; Pandey, M.; Deilmann, T.; Schmidt, P. S.; Hinsche, N. F.; Gjerding, M. N.; Torelli, D.; Larsen, P. M.; Riis-Jensen, A. C.; Gath, J.; Jacobsen, K. W.; Mortensen, J. J.; Olsen, T.; Thygesen, K. S. *2d Materials* **2018**, *5*

(9) Miao, N. H.; Xu, B.; Zhu, L. G.; Zhou, J.; Sun, Z. M. *Journal of the American Chemical Society* **2018**, *140*, 2417–2420

(10) Otrokov, M. M. et al. *Nature* **2019**, *576*, 416–+

(11) Tang, J.; Wu, Y. D.; Wang, W. W.; Kong, L. Y.; Lv, B. Y.; Wei, W. S.; Zang, J. D.; Tian, M. L.; Du, H. F. *Nature Nanotechnology* **2021**, *16*, 1161–1161

(12) Wang, W. W.; Song, D. S.; Wei, W. S.; Nan, P. F.; Zhang, S. L.; Ge, B. H.; Tian, M. L.; Zang, J. D.; Du, H. F. *Nature Communications* **2022**, *13*

(13) Uchoa, B.; Neto, A. H. C. *Physical Review Letters* **2007**, *98*

(14) Wiebe, C. R.; Janik, J. A.; MacDougall, G. J.; Luke, G. M.; Garrett, J. D.; Zhou, H. D.; Jo, Y. J.; Balicas, L.; Qiu, Y.; Copley, J. R. D.; Yamani, Z.; Buyers, W. J. L. *Nature Physics* **2007**, *3*, 96–100, Times Cited: 157 Wiebe, C. R. Janik, J. A. MacDougall, G. J. Luke, G. M. Garrett, J. D. Zhou, H. D. Jo, Y. -J. Balicas, L. Qiu, Y. Copley, J. R. D. Yamani, Z. Buyers, W. J. L. 168

(15) Sutou, Y.; Imano, Y.; Koeda, N.; Omori, T.; Kainuma, R.; Ishida, K.; Oikawa, K. *Applied Physics Letters* **2004**, *85*, 4358–4360

(16) Feng, Y.; Vaghefi, P. M.; Vranjkovic, S.; Penedo, M.; Kappenberger, P.; Schwenk, J.; Zhao, X.; Mandru, A. O.; Hug, H. J. *Journal of Magnetism and Magnetic Materials* **2022**, *551*

(17) Gross, B.; Philipp, S.; Josten, E.; Leliaert, J.; Wetterskog, E.; Bergstr?m, L.; Poggio, M. *Physical Review B* **2021**, *103*

(18) Weber, D.; Ruffer, D.; Buchter, A.; Xue, F.; Russo-Averchi, E.; Huber, R.; Berberich, P.; Arbiol, J.; Fontcuberta i Morral, A.; Grundler, D. *Nano letters* **2012**, *12*, 6139–6144

(19) Yu, Y.; Xu, F.; Wang, N.; Zou, L. K.; Xue, F. *Japanese Journal of Applied Physics* **2018**, *57*

(20) Peng, Y.; Ding, S.; Cheng, M.; Hu, Q.; Yang, J.; Wang, F.; Xue, M.; Liu, Z.; Lin, Z.; Avdeev, M.; Hou, Y.; Yang, W.; Zheng, Y.; Yang, J. *Advanced Materials* **2020**, *32*, 2001200

(21) Calder, S.; Haglund, A. V.; Liu, Y.; Pajerowski, D. M.; Cao, H. B.; Williams, T. J.; Garlea, V. O.; Mandrus, D. *Physical Review B* **2020**, *102*

(22) Joe, M.; Lee, H.; Aly?r k, M. M.; Lee, J.; Kim, S. Y.; Lee, C.; Lee, J. H. *Journal of Physics: Condensed Matter* **2017**, *29*, 405801

(23) Son, J. et al. *ACS Nano* **2021**, *15*, 16904–16912

(24) Lee, M. J.; Lee, S.; Lee, S.; Balamurugan, K.; Yoon, C.; Jang, J. T.; Kim, S. H.; Kwon, D. H.; Kim, M.; Ahn, J. P.; Kim, D. H.; Park, J. G.; Park, B. H. *Npg Asia Materials* **2018**, *10*

(25) Qi, S. M. et al. *Nature Communications* **2023**, *14*

(26) Yang, J. et al. *Physical Review Applied* **2021**, *16*

(27) Balan, A. P.; Kumar, A.; Scholz, T.; Lin, Z. C.; Shahee, A.; Fu, S.; Denneulin, T.; Vas, J.; Kov cs, A.; Dunin-Borkowski, R. E.; Wang, H. I.; Yang, J. B.; Lotsch, B. V.; Nowak, U.; Kl?ui, M. *Acs Nano* **2024**, *18*, 8383–8391